Formulation of electron motion in a storage ring with a betatron tune varying with time and a dipole shaker working at a constant frequency

Toshihiko Hiraiwa,[1,*] Kouichi Soutome,[2,1] and Hitoshi Tanaka[1]

[1]*RIKEN SPring-8 Center (RSC), Sayo, Hyogo 679-5148, Japan*

[2]*Japan Synchrotron Radiation Research Institute (JASRI), Sayo, Hyogo 679-5198, Japan*

(Received 2 September 2021; accepted 11 October 2021; published 2 November 2021)

In order to reduce the beam density efficiently for a safe beam abort, we analytically studied the motion of an aborted electron beam undergoing a sinusoidal kick by a beam shaker working at a constant frequency. Since the rf power is switched off, the betatron tune changes gradually with time due to chromatic effects. Chromatic aberration, together with a finite energy spread, enhances the dilution effect of the beam density, while the change in betatron tune with time causes a phase slippage that suppresses the growth of oscillation amplitude by the beam shaker. In order to treat such a situation properly, we formulated the motion of an aborted electron beam, taking into account nonlinear chromatic effects, under the adiabatic condition that the change in betatron tune is much slower than the betatron oscillation. In addition, by considering the case of a linearly varying betatron tune, it is shown that the response of an aborted electron beam can be interpreted as a superposition of waves, i.e., diffraction of waves. Our investigation not only provides a criteria for the determination of shaker's frequency for a safe beam abort but also has applications to resonance crossing phenomena.

DOI: 10.1103/PhysRevAccelBeams.24.114001

I. INTRODUCTION

In an electron storage ring, the stored electron beam is usually aborted by turning off the rf power for acceleration. The electron beam then loses its energy turn-by-turn by synchrotron radiation and eventually hits the inside of vacuum chambers. The energy of the electron beam is dissipated as heat by generating electromagnetic showers. The advantage of such an abort procedure is that it does not require an extra beam dump in the ring, which means the procedure is space effective and easy in ring design and in operation.

The beam abort procedure described above is effective only when the electron beam density is low enough not to damage vacuum chambers. In recent diffraction-limited light sources [1–6], where very high-density low-emittance beams are stored in vacuum chambers with a small cross section, the situation is expected to be much more severe, and therefore it is important to establish a safe abort procedure of high-density beams [5–9]. Tracking simulations anticipate that an aborted beam with the rf power turned off will strike a vacuum chamber with its density intact, causing the temperature of the chamber surface to rise above the melting point. As a matter of fact, even in a third-generation light source, where the vertical emittance already reaches the diffraction limit, there was an accident that the aborted beam melted the vacuum chamber [10].

In order to abort such high-density beams safely and protect vacuum chambers, we propose the following two countermeasures, in addition to the usual beam abort procedure. The first is to reduce the beam density in the vertical phase space by increasing the amplitude of betatron oscillation by a beam shaker in combination with the dilution effect of the beam density due to chromatic effects. Since, in the case of an usual storage ring with high superperiodicity, the time it takes for the aborted beam to hit the vacuum chamber is equal to or longer than the time it takes for the beam to be diffused in the phase space due to chromatic effects, the beam density can be sufficiently reduced with this method before the beam getting lost. The second is to install graphite beam absorbers with a high-melting point and a long radiation length at dispersive sections to absorb the vertically spread electron beam. These countermeasures prevent high-density beams from hitting vacuum chambers directly and ensure a safe beam abort. In the 3 GeV light source project [11], which is currently under construction, we adopt the above aborted beam handling system.

The reason for spreading the electron beam in the vertical phase space is as follows. With the rf power turned off, the beam orbit at dispersive sections shifts inward. Thereby, the electron beam is gradually scraped from the inside by

*hiraiwa@spring8.or.jp

the absorbers and eventually disappears. Spreading the electron beam horizontally increases the duration time from when the beam starts hitting the absorbers to when it disappears. The increase of the duration time is, however, more than one order of magnitude smaller than the thermal diffusion rate of the absorbers, and does not make any sense. On the other hand, spreading the electron beam vertically increases the contact area with the absorbers and thus reduces the beam density effectively.

During the beam abort process, the betatron tune of an electron beam varies gradually due to chromatic effects as the electron beam loses its energy turn-by-turn by synchrotron radiation. In this case, it is not trivial which frequency is most effective for spreading the electron beam in the phase space, and how much the beam density can be decreased. In order to systematically and efficiently study the beam density control by an external sinusoidal kick with a constant frequency, we formulated an equation of motion for an aborted electron beam undergoing a sinusoidal force, and solved it analytically by using a Green function method. The derived solution is valid under the adiabatic condition that the tune variation with time is much slower than betatron oscillation. It can also treat nonlinear chromatic effects as long as the adiabatic condition is satisfied.

The paper is organized as follows. In Sec. II, the motion of an aborted electron beam undergoing an external sinusoidal force is modeled, and an analytical expression is derived. In Sec. III, the growth and frequency response of the oscillation amplitude are numerically evaluated in our model and are compared to those obtained from tracking simulations to validate our model. In Sec. IV, we discuss the impact of the decoherence effect of betatron motion on the beam density. In Sec. V, we apply a linear approximation to the chromaticity to simplify our model, and discuss analogies between the beam motion and diffraction of light. The paper ends with a summary in Sec. VI.

II. FORMULATION OF THE ABORTED BEAM MOTION WITH A SINUSOIDAL FORCE

Let us consider the transverse motion of an aborted electron undergoing a sinusoidal kick by a beam shaker. Suppose that the beam shaker is placed at $s = s_f$ and applies a sinusoidal kick to an aborted electron beam every turn. Then, the transverse motion of an aborted electron is determined by the following inhomogeneous equation

$$\frac{d^2z}{ds^2} + K(s)z = F(s), \tag{1}$$

with an external force by the shaker

$$F(s) = \delta(s - s_f)F_0 \cos(2\pi\nu_f s/C), \tag{2}$$

where z stands for a transverse coordinate x or y, $K(s)$ is a periodic focusing function $K(s + C) = K(s)$ with a period C of the circumference, and ν_f is the frequency of the sinusoidal force (the number of oscillation during one turn of an electron).

The Courant-Snyder transformation [12] allows us to transform Eq. (1) into a quite familiar form, i.e., the equation of motion for a forced harmonic oscillator

$$\frac{d^2u}{d\phi^2} + \nu^2 u = \bar{F}(\phi). \tag{3}$$

Here, we introduce a normalized coordinate variable

$$u = \frac{z}{\sqrt{\beta}}, \tag{4}$$

and a new independent variable

$$\phi = \frac{1}{\nu}\int_0^s \frac{ds'}{\beta(s')}, \tag{5}$$

where ν is the betatron tune and $\beta(s)$ is the beta function. The external force $F(s)$ is transformed as

$$\begin{aligned}\bar{F}(\phi) &= \nu^2\beta^{3/2} \times \left|\frac{ds}{d\phi}\right|^{-1} \\ &\quad \times \sum_{0\le\phi_{f,n}\le\phi} \delta(\phi - \phi_{f,n})F_0 \cos(\nu_f\phi + \phi_0) \\ &= \nu\sqrt{\beta} \times \sum_{0\le\phi_{f,n}\le\phi} \delta(\phi - \phi_{f,n})F_0 \cos(\nu_f\phi + \phi_0) \\ &\equiv \sum_{0\le\phi_{f,n}\le\phi} \delta(\phi - \phi_{f,n})\bar{F}_0 \cos(\nu_f\phi + \phi_0),\end{aligned} \tag{6}$$

where $\phi_{f,n}$ denotes the phase function value at shaker's position every turn and $\bar{F}_0 \equiv \nu\sqrt{\beta}F_0$ is introduced.

Now, let us take into account the chromatic effects in Eq. (3) as a change in betatron tune with time. Then ν is an arbitrary function of ϕ and Eq. (3) becomes

$$\ddot{u} + \nu^2(\phi)u = \bar{F}(\phi). \tag{7}$$

Note that ν's in Eqs. (5) and (6) can be approximately replaced with a constant value ν_0, where ν_0 is the betatron tune at which the rf power is switched off ($\phi = 0$ or $t = 0$), for the following reason. Since the linear chromaticity for an ordinary storage ring has a small positive value, the adiabatic condition is in general satisfied; that is, the variation of the betatron tune due to synchrotron radiation is very slow compared to the betatron oscillation,

$$|\dot{\nu}(\phi)| \ll \nu^2(\phi) \quad \text{and} \quad |\ddot{\nu}(\phi)| \ll \nu^3(\phi). \tag{8}$$

Under the adiabatic condition of Eq. (8), the equation of motion (7) can be analytically solved with the help of the Green function method. According to Ref. [13], the Green function for Eq. (7) is given by

$$G(\phi,\phi') = \frac{-i}{2\sqrt{\nu(\phi)\nu(\phi')}} \exp\left[i\int_{\phi'}^{\phi}\nu(\chi)d\chi\right] + \text{c.c.} \quad (9)$$

With the Green function of Eq. (9), we have a particular solution for the equation of motion (7)

$$\begin{aligned} u(\phi) &= \int_0^{\phi} G(\phi,\phi')\bar{F}(\phi')d\phi' \\ &= \frac{i\bar{F}_0}{4\sqrt{\nu(\phi)}} \exp\left[-i\int_0^{\phi}\nu(\chi)d\chi\right] \times h(\phi;\nu_f) + \text{c.c.}, \end{aligned} \quad (10)$$

where $h(\phi;\nu_f)$ is an envelope function defined as

$$\begin{aligned} h(\phi;\nu_f) &= \sum_{0\le\phi_{f,n}\le\phi} \frac{1}{\sqrt{\nu(\phi_{f,n})}} \exp\left[i\int_0^{\phi_{f,n}}\nu(\chi)d\chi\right] \\ &\quad \times \left(e^{-i\nu_f\phi_{f,n}-i\phi_0} + e^{i\nu_f\phi_{f,n}+i\phi_0}\right) \\ &\approx \sum_{0\le\phi_{f,n}\le\phi} \frac{1}{\sqrt{\nu(\phi_{f,n})}} \exp\left[i\int_0^{\phi_{f,n}}\nu(\chi)d\chi\right] \\ &\quad \times \exp\left[-i(\nu_f\phi_{f,n}+\phi_0)\right] \\ &\approx \frac{1}{2\pi}\int_0^{\phi}\frac{d\phi'}{\sqrt{\nu(\phi')}} \\ &\quad \times \exp\left[i\left\{\int_0^{\phi'}\nu(\chi)d\chi - \nu_f\phi' - \phi_0\right\}\right]. \end{aligned} \quad (11)$$

Here, we neglect the rapidly oscillating terms (i.e., the second term of the first line), and replace the summation over $\phi_{f,n}$ with the integral. Note that the replacement of the summation with the integral is valid because the interval of $\phi_{f,n}$ $(=2\pi)$ is small enough compared to the oscillation period of the integrand (i.e., $|\nu-\nu_f| \ll 1$).

It is worth noting that, as discussed in Ref. [13], a similar expression to Eq. (10) can be also derived in the case where the betatron tune is kept constant while shaker's frequency varies. In this case, adiabatic condition such as Eq. (8) is not required to obtain an analytical solution.

III. COMPARISON TO PARTICLE TRACKING SIMULATION

In Sec. II, by means of simple modeling, we derived an analytical expression for the time evolution of betatron oscillation excited by an external sinusoidal force with a constant frequency. Here, we present how well the derived expression agrees with precise three-dimensional tracking simulations in the region where the adiabatic condition of Eq. (8) is satisfied.

Table I shows the machine parameters of the storage ring used for the comparison. Here we take, as an example, the storage ring of the 3 GeV light source project [11]. For tracking simulations, we use the tracking code, CETRA [14],

TABLE I. Machine parameters of the storage ring for the 3 GeV light source project [11]. The lattice is a four-bend achromat type. The capital letters H, V, and L in the table represent horizontal, vertical, and longitudinal, respectively.

Parameter	Value
Beam energy	3 GeV
Stored current	400 mA
Circumference	348.8 m
rf frequency	508.76 MHz
rf voltage	3.6 MV
Synchrotron tune	0.00695
Harmonic number	592
Number of cells	16
Natural emittance	1.14 nmrad
Betatron tune	28.17 (H)/9.23 (V)
Energy spread	0.0843%
Momentum compaction Factor	4.33e-4
Bending field	0.869 T
Radiation loss (by bending magnets)	0.62 MeV/turn
Damping partition number	1.39(H)/1.00(V)/1.61(L)
Damping time (ms)	8.09(H)/11.24(V)/6.98(L)

which performs a symplectic integration [15,16] based on the Hamiltonian for the motion of a charged particle in the six-dimensional phase space without expanding its square-root form. The code can handle the couplings between betatron oscillations and path length changes. The cavity and the fringe field of magnets are treated in the thin-lens approximation [17]. Since the effect of radiation fluctuations is small, the calculations shown below use the expected value of the radiation to simulate the energy loss (i.e., fluctuations per radiation are averaged out).

In the ring for the 3 GeV light source project, the electron beam will start hitting the beam absorbers around the 400th turn after the rf power is turned off. Therefore, the electron beam density must be reduced sufficiently around the 400th turn. Moreover, in order to ensure sufficient time margin, the electron beam should be well spread out in the vertical phase space within the 300th turn.

Figure 1 shows the vertical betatron tune as a function of the number of turns after the rf power is turned off. The betatron tune varies gradually according to the nonlinear chromaticity with the energy loss due to synchrotron radiation. As we see in the figure, the betatron tune varies linearly up to the 100th turn, whereas nonlinearities show up after that. To be able to treat properly in our model the aborted beam motion at least up to the 300th turn after the rf power turned off, we take into account the nonlinear chromaticity up to the fifth order of the relative energy deviation, and fit the CETRA calculation by a fifth-degree polynomial function

$$\nu(\delta) = \nu_0 + \xi_1\delta + \xi_2\delta^2 + \xi_3\delta^3 + \xi_4\delta^4 + \xi_5\delta^5, \quad (12)$$

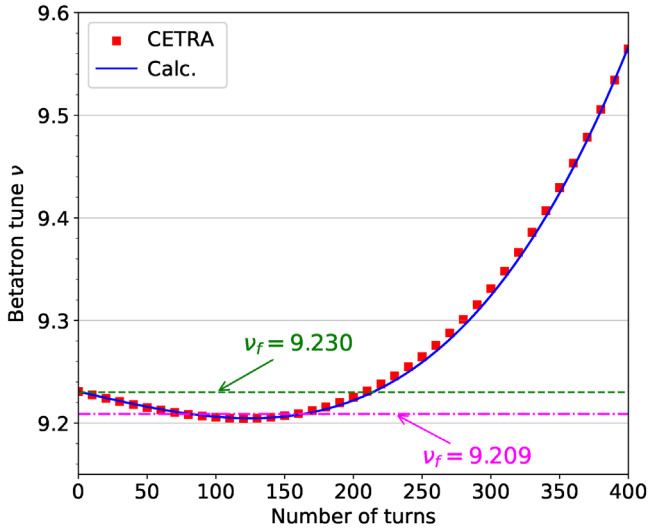

FIG. 1. Vertical betatron tune as a function of the number of turns after the rf is turned off. Red squares represent the CETRA calculation, while a blue solid curve represents the fit to the CETRA results with Eq. (12). Green dashed and magenta dash-dotted lines correspond to shaker's tune (frequency) $\nu_f = 9.230$ and $\nu_f = 9.209$, respectively.

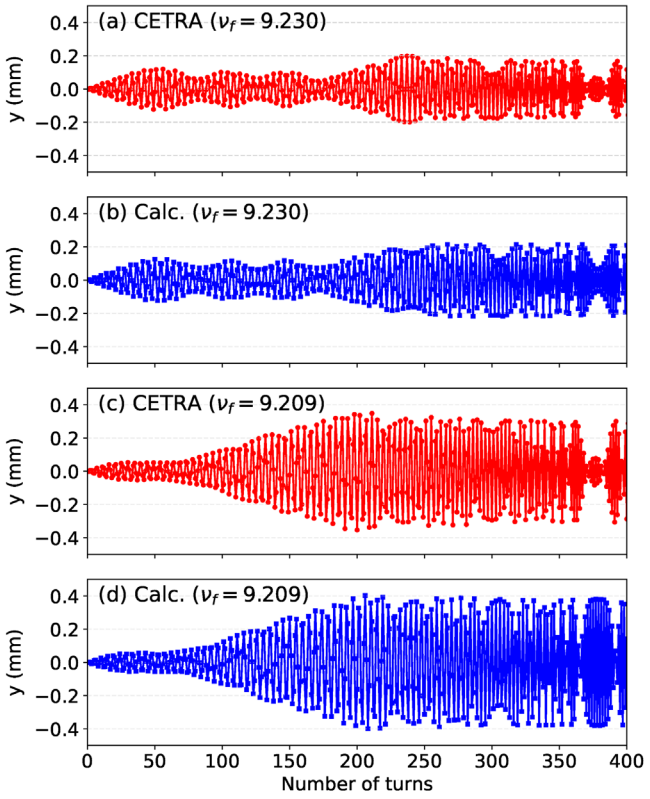

FIG. 2. Vertical betatron oscillation excited by the beam shaker at an observation point in the storage ring. (a) CETRA tracking and (b) model calculation with shaker's tune (frequency) $\nu_f = 9.230$, and (c) CETRA tracking and (d) model calculation with $\nu_f = 9.209$. In both cases, the initial amplitude of betatron oscillation is set to zero and the magnitude of shaker's kick is set to 2 μrad.

where $\delta = -n\Delta$ and $\Delta = U/E_0$ are defined, E_0 is the reference beam energy, U is the radiation loss per turn, and n is the number of turns after the rf power turned off. The fit result by Eq. (12), as shown in Fig. 1 as a blue solid curve, can well reproduce the CETRA calculation up to the 400th turn.

Figure 2 shows the comparison between the model calculation using Eq. (10) and tracking simulation of vertical betatron oscillation excited by the beam shaker up to the 400th turn at an observation point in the ring. Two different shaker's frequencies, corresponding to green dashed and magenta dash-dotted lines in Fig. 1, are examined. Though the model calculation is in excellent agreement with the CETRA tracking for both shaker's frequencies up to the 230th turn, we see some discrepancies between them after that. There are two possible reasons for the discrepancies. First, the CETRA tracking correctly handles the change in path length due to radiation loss, whereas the model calculation does not take such an effect into account. Therefore, in our model, as the number of turns increases, the timing of receiving a kick from the beam shaker will deviate from the actual timing. Second, as the number of turns increases, the rate of change in betatron tune becomes larger (see Fig. 1), and consequently the adiabatic approximation becomes poor.

From the analytical expression of betatron oscillation given by Eq. (10), the oscillation amplitude is written as

$$A(\phi;\nu_f) = \frac{\bar{F}_0}{4\sqrt{\nu(\phi)}} \times |h(\phi;\nu_f)|. \tag{13}$$

Thus, the envelope function $|h(\phi;\nu_f)|$ can be viewed as a frequency response of the oscillation amplitude at the nth turn [$n = \phi/(2\pi)$].

Figure 3 shows the frequency response $|h(\nu_f)|$ of the oscillation amplitude at the 400th turn with shaker's frequency ranging from 7.74 to 8.17 MHz, equivalently from 9.0 to 9.5 in terms of tune. For comparison, the oscillation amplitude at the 400th turn for several shaker's frequencies was calculated from single-particle tracking by CETRA and the results are overlaid in Fig. 3(b) as red squares. Our model well reproduces a complicated pattern of the frequency response. Although our model is very simple, it can predict the time evolution of the oscillation amplitude at an arbitrary shaker frequency without any time-consuming calculations.

For a given total number of turns, the total gain from the beam shaker is determined by two main factors. One is the number of times the aborted beam passes through the resonance condition. As we see in Fig. 3(a), we have almost no gain for $\nu_f \lesssim 9.20$. In this region, the aborted beam never crosses any resonance conditions (see also Fig. 1). On the other hand, for $9.20 \lesssim \nu_f \leq 9.23$, the aborted beam crosses the resonance condition twice, and thus we have

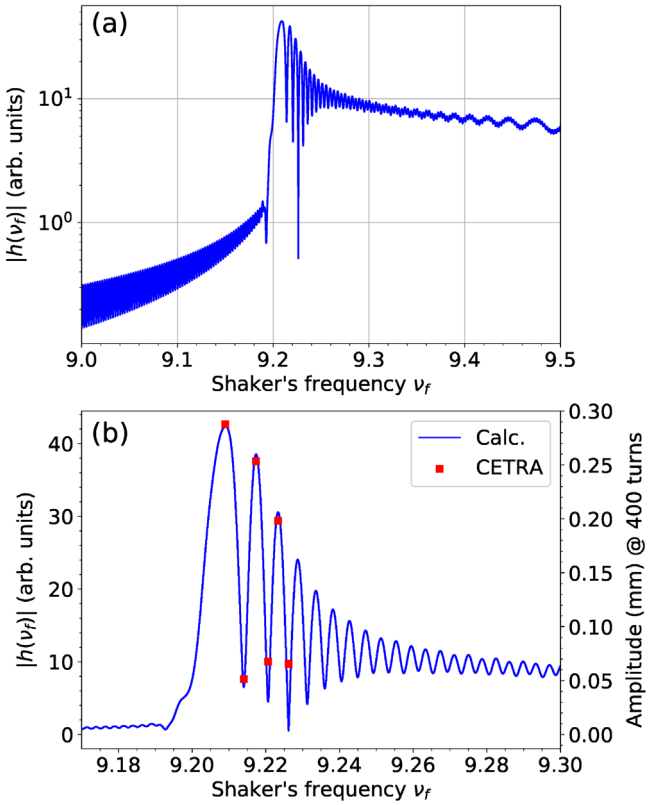

FIG. 3. Frequency response of the oscillation amplitude at the 400th turn. (a) The scale for the y axis is logarithmic. (b) The scale for the y axis is linear. Red squares represent the oscillation amplitude at the 400th turn calculated from single-particle tracking by CETRA.

more than twice as large as the total gain in the other region, where the aborted beam crosses the resonance condition only once ($\nu_f > 9.23$).

Another factor that determines the total gain is the speed at which the aborted beam passes through the resonance condition. As we shall see later, the time duration of gaining energy efficiently from the beam shaker is inversely proportional to the square root of the speed of crossing the resonance condition. Consequently, the oscillation amplitude after the resonance crossing is also proportional inversely to it. In fact, we have the maximum total gain at $\nu_f \approx 9.209$. In this case, the crossing speed is almost zero (see Fig. 1).

There is another point worth mentioning. Besides the gross structure of the frequency response discussed above, we see a characteristic ringing pattern. In particular, the total gain is quite low at $\nu_f \approx 9.214$, 9.221, and 9.226, even though the aborted beam crosses the resonance condition twice. Such a behavior can be understood by interpreting the integration in Eq. (11) as a superposition of waves in the frequency space, as discussed in Sec. V; that is, "wavepackets" coming from the first and second resonance crossings cancel each other. In fact, the difference between the phases of the integrand in Eq. (11) at the first and second resonance crossings, $\Delta\Phi$, can be approximately written as $\Delta\Phi \approx \pi \times (2m+1)$ (m: integer).

IV. DECOHERENCE OF BETATRON MOTION

The decoherence effect of betatron motion, as well as the growth of oscillation amplitude excited by the beam shaker, is a key issue to reduce the beam density for a safe beam abort. In this section, we discuss the impact of the decoherence effect of betatron motion on the beam density.

Figure 4 shows the (y, y') phase space distributions of 5000 particles in a single bunch excited by the beam shaker. The aborted beam, initially concentrated at the origin, is gradually stretched in the phase space due to the decoherence effect while the oscillation amplitude is increased by the beam shaker up to about the 100th turn. After that, the beam shrinks once [Fig. 4(c)] and then starts getting stretched again. Around the 300th turn, the phase space distribution becomes like a ring. The radius of the ring, i.e., the maximum oscillation amplitude of an electron, corresponds to ~200 μm, which is almost consistent with the result of single-particle tracking [see Fig. 2(a)].

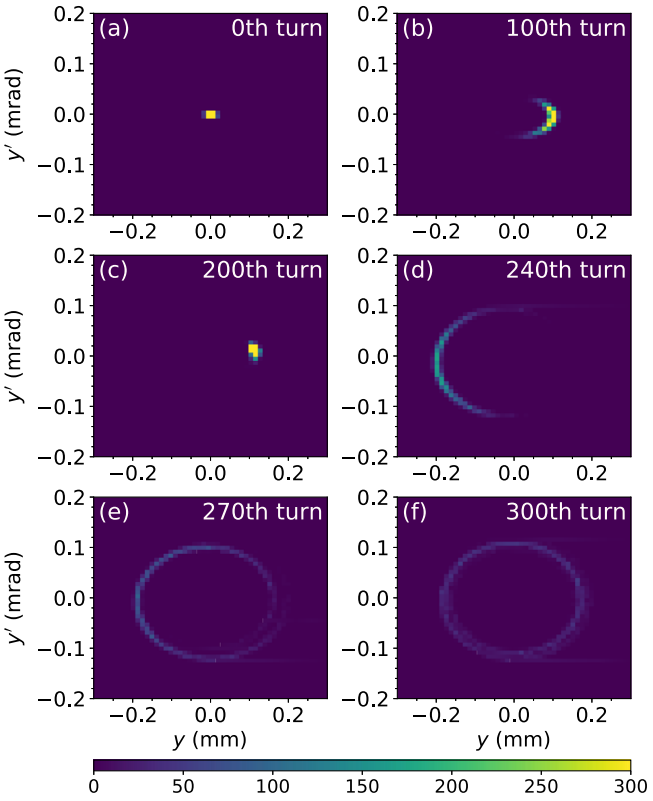

FIG. 4. (y, y') phase space distribution of 5000 particles in a single bunch (a) at the 0th, (b) 100th, (c) 200th, (d) 240th, (e) 270th, and (f) 300th turn, respectively, simulated by CETRA. In the simulation, the magnitude and the frequency of a sinusoidal kick are, respectively, set to 2 μrad and $\nu_f = 9.230$. In addition, the x-y coupling of 1% is introduced, assuming the actual ring condition.

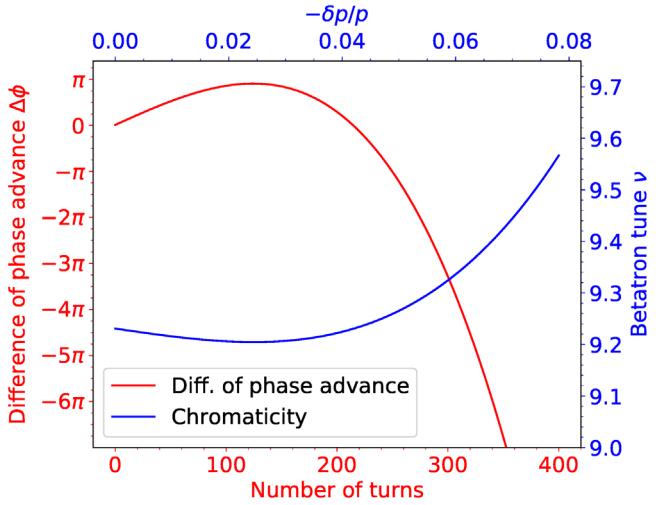

FIG. 5. Difference of the phase advances between high momentum [$\delta p/p = +0.17\%$ ($+2\sigma$)] and low momentum [$\delta p/p = -0.17\%$ (-2σ)] particles (red curve, bottom and left axes) and the chromaticity for vertical motion (blue curve, top and right axes).

Thanks to the decoherence effect together with the perturbation by the beam shaker, the beam density can be reduced by a factor of ~300 in the present case.

The behavior of the phase space distribution described above can be well explained by the energy spread and the chromaticity. Figure 5 shows the difference of the phase advances between high momentum ($\delta p/p = +0.17\%$, corresponding to a $+2\sigma$ deviation) and low momentum ($\delta p/p = -0.17\%$, corresponding to a -2σ deviation) particles in a single bunch, together with the chromaticity for vertical motion. Up to the 125th turn, the phase advance difference increases monotonically according to the linear chromaticity. Then, it decreases due to the nonlinear chromaticity and crosses zero around the 200th turn. After that, as the nonlinearities of chromaticity increase, the phase advance difference becomes larger and larger in the negative direction, reaching -2π at around the 270th turn. It is obvious from the above discussion that the decoherence time, i.e., the time it takes for the aborted beam to fill the phase space in a ring, depends on the energy spread and the nonlinearities of chromaticity. It should be noted that the aborted beam does not undergo synchrotron oscillation because of the rf power switched off.

Storage ring light sources usually operate in a multibunch mode. In this case, the dilution effect of the beam density is further enhanced because the initial phase of betatron oscillation excited by a beam shaker is different for each bunch.

V. LINEARLY VARYING TUNE AND ANALOGIES TO LIGHT DIFFRACTION

To understand the behavior of the frequency response, as discussed in Sec. III, in more detail, we hereafter restrict ourselves to the simplest case; namely, the betatron tune varies linearly as

$$\nu(\delta) = \nu_0 + \xi_1\delta = \nu_0 - \xi_1\Delta\frac{\phi}{2\pi} \equiv \nu(\phi), \tag{14}$$

where $\xi_1\Delta > 0$.

As discussed in Ref. [13], a forced harmonic oscillator with a slowly varying natural frequency is essentially equivalent to light diffraction. Just as the intensity pattern of light diffraction from a single slit varies with the Fresnel number N_F from a Fraunhofer pattern ($N_F \ll 1$) to a Fresnel one ($N_F \gtrsim 1$), the frequency response of the oscillation amplitude changes its behavior according to the corresponding Fresnel number $\bar{N}_F$. In the present case, the Fresnel number $\bar{N}_F$ is given by

$$\bar{N}_F = \frac{\xi_1\Delta}{4}\left(\frac{\phi}{2\pi}\right)^2. \tag{15}$$

Using the above Fresnel number, one can easily estimate the frequency response with a quite simple calculation.

Still following the discussion in Ref. [13], let us consider the growth of the betatron amplitude (or the envelope function $|h|$), starting at $\nu(0) = \nu_f$ (i.e., we choose $\nu_f = \nu_0$). From Eq. (11), the amplitude growth $h(\phi)$ in this case is written as

$$h(\phi;\nu_f = \nu_0) \approx \frac{e^{-i\phi_0}}{\sqrt{2\nu_0\xi_1\Delta}}\left[C\left(\sqrt{2\xi_1\Delta}\frac{\phi}{2\pi}\right) - iS\left(\sqrt{2\xi_1\Delta}\frac{\phi}{2\pi}\right)\right], \tag{16}$$

where two functions $C(x)$ and $S(x)$ are the so-called Fresnel integrals

$$C(x) = \int_0^x \cos\left(\frac{\pi}{2}w^2\right)dw \quad \text{and} \tag{17}$$

$$S(x) = \int_0^x \sin\left(\frac{\pi}{2}w^2\right)dw. \tag{18}$$

Figure 6 shows the growth of the betatron amplitude as given by Eq. (16). We see that the growth of the betatron amplitude behaves like an intensity pattern of knife-edge diffraction (i.e., Fresnel diffraction from a straight edge).

As we see in Fig. 6, the betatron amplitude increases monotonically until a certain number of turns, $\delta\phi/(2\pi)$, then it starts beating and asymptotically converges to a certain value, $|h|_\infty$. These quantities can be evaluated by using the analogies together with our knowledge of light diffraction (see Ref. [13] for detail discussion)

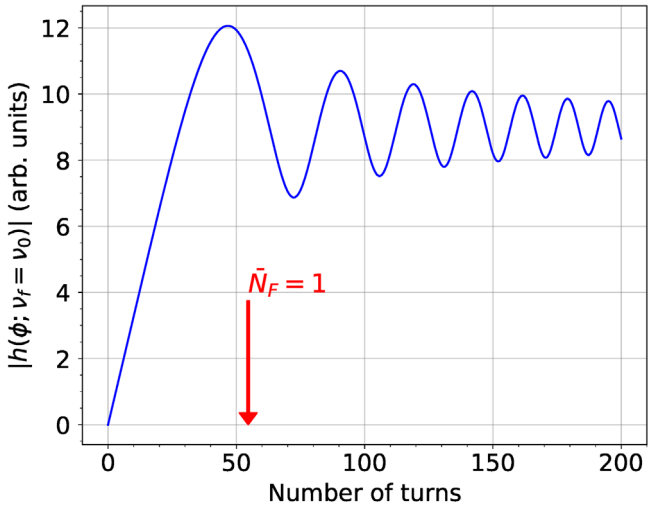

FIG. 6. Amplitude growth of betatron oscillation, starting at $\nu(0) = \nu_f$. The machine parameters used in the calculation are the same as those of Sec. III, except that the chromaticity is linearized. A red arrow indicates the number of turns $[= \delta\phi/(2\pi)]$ corresponding to $\bar{N}_F = 1$ (see the text and Ref. [13] for details).

$$\frac{\delta\phi}{2\pi} = \frac{1}{\sqrt{\xi_1\Delta}} \quad \text{and} \tag{19}$$

$$|h|_\infty = \frac{1}{2\sqrt{\nu_0\xi_1\Delta}}. \tag{20}$$

Our conclusion that the asymptotic amplitude is inversely proportional to the square root of the crossing speed $\xi_1\Delta$ agrees with the previous study on integer-resonance crossing [18].

In what follows, to see the nonlinear chromatic effects on the frequency response, we focus on the range from the 215th to 400th turn, where the betatron tune crosses the resonance condition once and where the nonlinear effects are rather large (see Fig. 1), and calculate the frequency response for the following two cases. The one is the case where the betatron tune varies according to Eq. (12), and the other is the case where the betatron tune varies linearly. For comparison, the total change in betatron tune is set to be the same in both cases (i.e., the rate of change in betatron tune is averaged out in the linear case), as shown in Fig. 7. The results are compared in Fig. 8.

For the linear case, the parameters used in the calculation give the Fresnel number $\bar{N}_F \approx 16.5$, so the frequency response exhibits a Fresnel diffraction pattern. In the light diffraction theory, a Fresnel diffraction pattern represents just a shape of the slit aperture, and a ripple structure on the plateau comes from constructive or destructive interference between the incident plane wave and the diffracted wave (i.e., the secondary spherical wave) from the aperture edge [19]. Because of a quadratic change in optical path length difference under the Fresnel approximation, the spatial

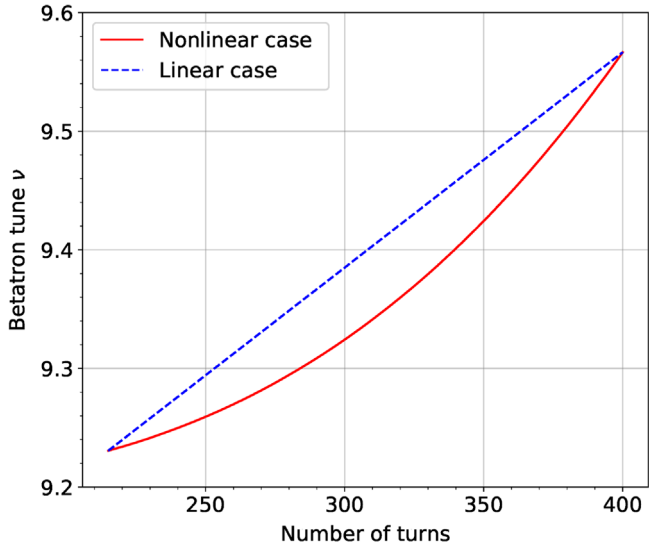

FIG. 7. Tune excursion from 215 to 400 turns. A red solid curve redraws Fig. 1, whereas a blue dashed line represents a linearized one.

frequency of the ripple structure becomes higher toward the center. Using the concept of Fresnel zones, the position of a dip as measured from the aperture edge is approximately written as $\sqrt{(2m-1)\lambda r_0}$ $(m = 1, 2, \ldots)$, where λ and r_0 are the wavelength and the slit-screen distance, respectively, and $m = 1$ represents the first dip from the edge. Thus, by applying the correspondence relation given in Ref. [13] to the present case, the range of resonant frequencies almost coincides with the range in which the betatron tune varies,

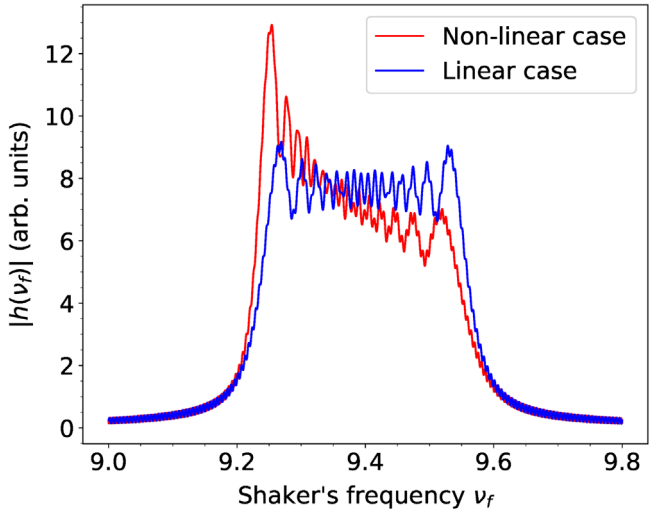

FIG. 8. Comparison of the frequency responses for the range from the 215th to 400th turn with and without the nonlinear chromatic effects. Red and blue curves represent the nonlinear and linear cases, respectively. The machine parameters for the nonlinear case are the same as those of Sec. III, whereas the calculation for the linear case uses the averaged chromaticity parameters (see the text for details).

and the spacing of ripple peaks is determined by the crossing speed $\xi_1\Delta$.

Looking at the nonlinear case, on the other hand, the frequency response exhibits a Fresnel-like but asymmetrical pattern; that is, as shaker's frequency ν_f increases, the peak height decreases gradually and the width of a ripple peak becomes wider. These deformation can be accounted for by the nonlinear chromatic effects. For example, from Eq. (20), the ratio of the square root of the crossing speed $\xi_1\Delta$ at $\nu_f = 9.252$ and 9.515, corresponding to the pronounced peaks at the both edges, is $\sqrt{1.5/4.8} \approx 0.56$, in good agreement with the ratio of $|h|$ obtained from the figure, $7.0/13.0 \approx 0.54$. The increasing width of a ripple peak with ν_f can be also understood in terms of the change of the crossing speed $\xi_1\Delta$. Note that the number of ripple peaks is the same for both the nonlinear and linear cases, and therefore, even in the nonlinear case, the Fresnel number $\bar{N}_F$ can be defined by linearizing the chromaticity parameters.

Returning back to the discussion of the characteristic behavior shown in Fig. 3, it can be viewed as a further superposition of two diffraction patterns with different Fresnel numbers $\bar{N}_F$—one corresponding to the range from 0 to 125 turns and the other to the range from 126 to 400 turns (see Fig. 1).

VI. SUMMARY

In diffraction-limited light sources, it is crucial to abort the stored electron beam safely. For this purpose, we constructed a simple model for an aborted electron beam undergoing an external sinusoidal kick with a constant frequency. The model can treat nonlinear chromatic effects as long as the betatron tune varies slowly enough compared to betatron oscillation. It was demonstrated that the model can predict the growth of the oscillation amplitude at an arbitrary shaker's frequency under the adiabatic condition, and thus serves well for a quick estimate of the frequency response. In addition, to understand a characteristic behavior of the frequency response obtained from the model, we simplified the model to the case of a linearly varying tune, and showed that it can be interpreted as a superposition of waves in the frequency space and can be discussed in the same manner as light diffraction. Our investigation not only facilitates the design of a beam-abort system in a diffraction-limited ring but may also shed light on another aspects of resonance-crossing phenomena.

[1] SPring-8-II Conceptual Design Report (2014), http://rsc.riken.jp/pdf/SPring-8-II.pdf.

[2] EBS Storage Ring Technical Report (2018), https://www.esrf.fr/about/upgrade.

[3] Y. Jiao *et al.*, The HEPS project, J. Synchrotron Radiat. **25**, 1611 (2018).

[4] L. Liu *et al.*, Sirius commissioning results and operation status, in *Proceedings of IPAC2021* (2021), p. 13.

[5] Advanced Photon Source Upgrade Project Preliminary Design Report, Argonne National Laboratory, Report No. aPSU-2.01-RPT-002, 2017.

[6] C. G. Schroer *et al.*, PETRA IV: Upgrade of PETRA III to the ultimate 3D x-ray microscope, Conceptual Design Report, 2019, https://doi.org/10.3204/PUBDB-2019-03613.

[7] M. Borland *et al.*, Using decoherence to prevent damage to the swap-out dump for the APS upgrade, in *Proceedings of IPAC2018* (2018), p. 1494.

[8] M. Borland *et al.*, Simulation of beam aborts for the Advanced Photon Source to probe material-damage limits for future storage rings, in *Proceedings of NAPAC2019* (2019), p. 106.

[9] J. Dooling *et al.*, Studies of beam dumps in candidate horizontal collimator materials for the Advanced Photon Source upgrade storage ring, in *Proceedings of NA-PAC2019* (2019), p. 128.

[10] H. Tanaka *et al.*, Top-up operation of SPring-8 storage ring with low-emittance optics, in *Proceedings of EPAC2006* (2006), p. 3359.

[11] N. Nishimori, T. Watanabe, H. Tanaka *et al.*, A highly brilliant compact 3 GeV light source project in Japan, in *Proceedings of IPAC2019* (2019), p. 1478.

[12] E. Courant and H. Snyder, Theory of the alternating-gradient synchrotron, Ann. Phys. (N.Y.) **3**, 1 (1958).

[13] T. Hiraiwa, K. Soutome, and H. Tanaka, Forced harmonic oscillator interpreted as diffraction of light, Phys. Rev. E **102**, 032211 (2020).

[14] J. Schimizu *et al.*, Development of a tracking and analysis code for beam dynamics in SPring-8, in *Proceedings of the 13th Symposium on Accelerator Science and Technology* (2001), p. 80.

[15] H. Yoshida, Construction of higher order symplectic integrators, Phys. Lett. A **150**, 262 (1990).

[16] H. Yoshida, Recent progress in the theory and application of symplectic integrators, Celestial Mech. Dyn. Astron. **56**, 27 (1993).

[17] E. Forest *et al.*, The correct local description for tracking in rings, Part. Accel. **45**, 65 (1994).

[18] J. LeDuff, Integer resonance crossing in H. I. accumulator ring, in *Proceedings of Heavy Ion Fusion Workshop* (1979), p. 310.

[19] M. Born and E. Wolf, *Principles of Optics*, 7th ed. (Cambridge University Press, Cambridge, England, 2019).